Spark plasma sintering of Mn–Al–C hard magnets

Alexandre Pasko, Martino Lobue, E. Fazakas, L. K. Varga, Frederic Mazaleyrat

Spark plasma sintering of Mn-Al-C hard magnets

A Pasko[1], M LoBue[1], E Fazakas[2], L K Varga[2] and F Mazaleyrat[1]

[1] SATIE, ENS Cachan, CNRS, UniverSud Paris, F-94235 Cachan, France
[2] ISSPO, Wigner RCP, HAS, H-1525 Budapest, POB 49, Hungary

E-mail: pasko@satie.ens-cachan.fr

Abstract. Structural and magnetic characterization of isotropic Mn-Al-C bulk samples obtained by spark plasma sintering (SPS) is reported. This technique, to our knowledge, has not been used for preparation of Mn-Al-based permanent magnets yet. Transformation from the parent ϵ-phase to the ferromagnetic τ-phase occurred on heating in the process of sintering. The phase constitution of melt-spun precursors and consolidated samples was determined by X-ray diffraction. Magnetic hysteresis loops were recorded using a vibrating sample magnetometer. The compositional dependence of coercivity, magnetization and density of sintered materials is analyzed. To combine good magnetic properties with proper densification, further optimization of the production parameters is necessary.

PACS numbers: 75.50.Cc, 75.50.Ww, 75.60.Ej, 81.40.Rs

Submitted to: *J. Phys.: Condens. Matter*

1. Introduction

Mn-Al alloys are attractive candidates for permanent magnet applications due to reasonable magnetic properties, good technological properties (strength, workability, corrosion resistance) and low cost (no rare earth elements). With proper optimization, they would be capable of filling the gap between hard ferrites and Nd-Fe-B magnets [1]. The ferromagnetic tetragonal τ-phase with strong uniaxial magnetocrystalline anisotropy [2, 3] forms from the non-magnetic hexagonal ϵ-phase by annealing a quenched $Mn_{50+x}Al_{50-x}$ alloy ($x = 0 \dots 10$) at 400–700 °C. Both phases are metastable at room temperature and therefore need special thermal treatment. Carbon addition stabilizes τ-phase, increases coercivity, and facilitates production of enhanced anisotropic materials by hot deformation [4]. Magnetic hysteresis of Mn-Al-C alloys is sensitive to the microstructure and presence of defects developed during τ-phase formation, comprising martensitic or massive transformation mechanisms [5], and is therefore strongly influenced by the production route.

Various manufacturing techniques have been employed for preparation of homogeneous Mn-Al-C alloys: melt-spinning [6, 7, 8], levitation melting with splat quenching [9], spark erosion [10], ball milling [11, 12], mechanical grinding [13]. Depending on the solidification rate or size reduction degree, fine-grained materials

with improved functional properties can be obtained. In this paper we report on the structural and magnetic characterization of isotropic Mn-Al-C bulk samples produced by spark plasma sintering (SPS). This technique, to our knowledge, has not been used for preparation of Mn-Al-based permanent magnets yet. During SPS the heat is generated by a pulsed electric current passing directly through the powder compacted by a simultaneously applied uniaxial pressure [14]. The process is very fast and ensures full densification of nanosized powders at moderate temperatures without significant coarsening. Melt-spinning of the cast alloys is employed to make homogeneous ϵ-phase precursors with fine grains [15]. Transformation to the ferromagnetic τ-phase occurs on heating in the process of sintering. The goal is to investigate a correlation between the production route, phase constitution and resulting hard magnetic properties.

2. Experimental

Binary alloy $Mn_{55}Al_{45}$ and ternary compositions $Mn_{49}Al_{49}C_2$ and $Mn_{54}Al_{44}C_2$ doped with carbon were selected for the present study. The ingots prepared by induction melting were cast into ∼3 mm wide and ∼25 µm thick ribbons using a melt-spinning technique [7]. Brittle ribbons were subsequently milled by hand with pestle and mortar. The obtained powders were compacted in a graphite die with internal diameter of 8 mm and sintered in a Sumitomo Dr. Sinter Lab SPS machine under vacuum with applied pressure of 70 MPa. Thermal conditions were chosen as follows: maximum temperature from 650 to 950 °C, heating/cooling rate 100 K/min, dwell time 5 min (temperature was measured by a thermocouple inside the die). For comparison, the ribbons were also annealed either in a vacuum furnace at 550 °C for 10 min with ramping rate of 10 K/min or directly in the magnetometer cell. To ensure better densification, we increased the sintering temperature of ϵ-phase precursors. Crystal structures were examined in Co-K_α radiation by a PANalytical X'Pert Pro X-ray diffractometer (XRD) equipped with an X'Celerator linear detector. Full-profile analysis of XRD spectra was performed using a Rietveld-based software MAUD [16]. The density of sintered samples was measured by Archimedes method. Magnetization curves were recorded by a Lake Shore 7400 Series vibrating sample magnetometer (VSM) with a variable temperature assembly.

3. Results and discussion

3.1. Spark plasma sintering

The idea behind spark plasma sintering is simultaneous application of heat and pressure for more efficient consolidation of powders. Unlike hot pressing, SPS uses a resistive heating by a pulsed electric current passing directly through the die and (for conducting materials) the sample. This gives a number of advantages as the current can play an intrinsic role contributing to mass transport, and much higher heating rates can be achieved [14]. Materials are typically sintered in a matter of minutes as opposed to hours for conventional methods, and the temperatures needed for consolidation to full density are significantly lower, which open the possibility to create materials with nanoscale features [17]. In addition to rapid Joule heating, various mechanisms of observed enhanced sintering were proposed: local melting and evaporation, plasma formation between particles, cleaning effect due to removal of oxide films and adsorbed gases from the particle surface, enhanced diffusion at

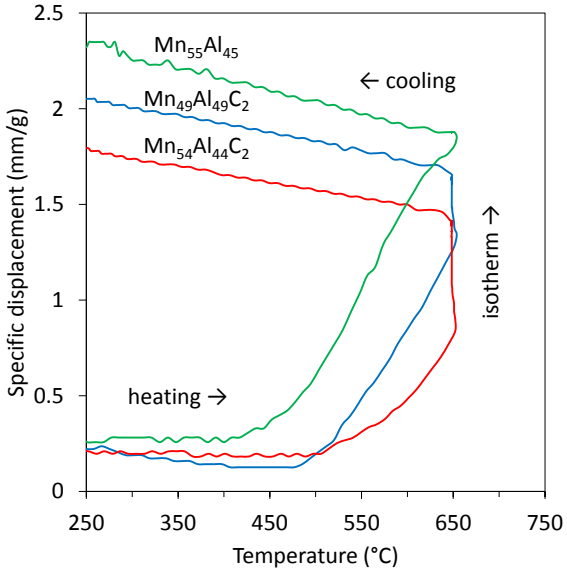

Figure 1. Displacement of the punch (expressed per powder mass) as a function of temperature during SPS. Isothermal sintering behaviour at 650 °C depends on the alloy composition.

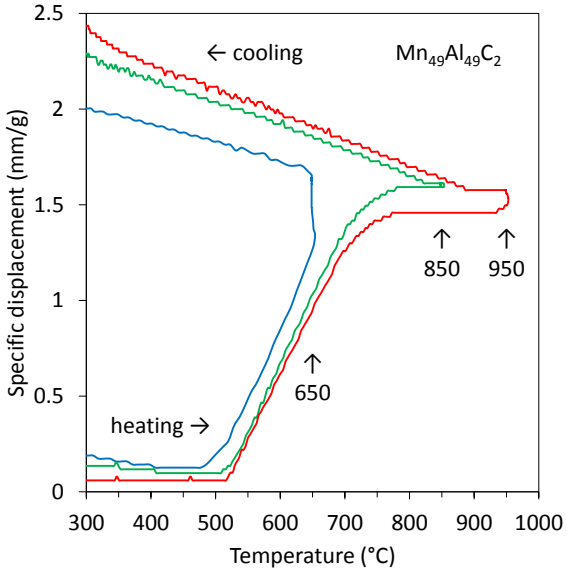

Figure 2. Displacement of the punch (expressed per powder mass) as a function of temperature during SPS for $Mn_{49}Al_{49}C_2$ alloy with isothermal stages indicated. Sintering is completed at ∼800 °C.

forming particle necks [18]. However, for many of these phenomena (especially those that invoke the presence of plasma) no unambiguous experimental evidence has been

reported [17].

As applied to synthesis of Mn-Al-C magnets, SPS technique can be beneficial to combine in one step the heat treatment necessary for τ-phase formation and the powder sintering itself, while avoiding excessive grain coarsening and decomposition of metastable phases in the intermediate temperature region. We tried two thermal regimes: at lower temperatures (650 °C) sintering is accompanied by $\epsilon \rightarrow \tau$ phase transition; at higher temperatures (850–950 °C) the material is sintered in the stable ϵ-phase state, and transformation to τ-phase occurs on cooling.

The SPS machine allows to record several important parameters controlling the process of sintering. Figure 1 shows the temperature dependence of the volume occupied by the powder in a die caused by application of heat and pressure. A sharp increase of the punch displacement on heating indicates the temperature at which sintering begins. Vertical segments of the curves correspond to the isothermal stage of sintering. The negative slope on cooling reflects a thermal contraction of densified samples. In $Mn_{55}Al_{45}$ alloy the powder consolidation starts at ∼450 °C and practically finishes before the isothermal stage. On the other hand, in $Mn_{49}Al_{49}C_2$ and $Mn_{54}Al_{44}C_2$ alloys the powder consolidation starts at ∼500 °C and continues during the isothermal stage. Among the three samples, $Mn_{54}Al_{44}C_2$ shows the longest isothermal sintering and the smallest total deformation. This behaviour can be explained by increasing stability of ϵ-phase in the sequence $Mn_{55}Al_{45} \rightarrow Mn_{49}Al_{49}C_2 \rightarrow Mn_{54}Al_{44}C_2$ to decomposition, as described below, and higher sintering ability of the equilibrium γ_2-phase. Figure 2 shows similar curves with different maximum temperatures. We can estimate that sintering of $Mn_{49}Al_{49}C_2$ alloy completes at ∼800 °C.

3.2. Phase analysis

Phase compositions of melt-spun ribbons (as-quenched and annealed) and sintered bulk samples have been determined by XRD. According to the phase diagram of Al-Mn system [19], formation of two equilibrium phases is expected: Mn-rich disordered cubic β-phase and Al-rich ordered trigonal γ_2-phase. In addition, two metastable phases may appear in non-equilibrium conditions: disordered hexagonal ϵ-phase and ordered tetragonal τ-phase. Stable at higher temperatures, ϵ-phase can be preserved on quenching and transformed into ferromagnetic τ-phase by a composition-invariant (involving only short-range diffusion) structural transition. Depending on the initial chemical composition and thermal history, all these phases were observed in different combinations. Figure 3 presents XRD spectra from the precursor powders, whereas figure 4 shows them after spark plasma sintering at 550 °C (some weak unreferenced peaks belong to the identified phases).

Some results of quantitative phase analysis based on Rietveld refinement of XRD data are presented in table 1. Weight fractions and lattice parameters of observed crystal structures have been determined. The melt-spun $Mn_{55}Al_{45}$ and $Mn_{54}Al_{44}C_2$ alloys enriched in Mn are composed entirely of ϵ-phase, whereas $Mn_{49}Al_{49}C_2$ composition contains also significant amount of γ_2-phase. The effect of subsequent heat treatment depends on the presence of carbon. In the binary $Mn_{55}Al_{45}$ alloy ϵ-phase decomposes completely into a pair of equilibrium γ_2-phase and β-phase. In the ternary $Mn_{49}Al_{49}C_2$ and $Mn_{54}Al_{44}C_2$ alloys ϵ-phase transforms on heating into ferromagnetic τ-phase. However, certain quantity of γ_2-phase is always detected (the rest is Mn_3AlC not given in the table). On the other hand, we obtain 100 % τ-phase

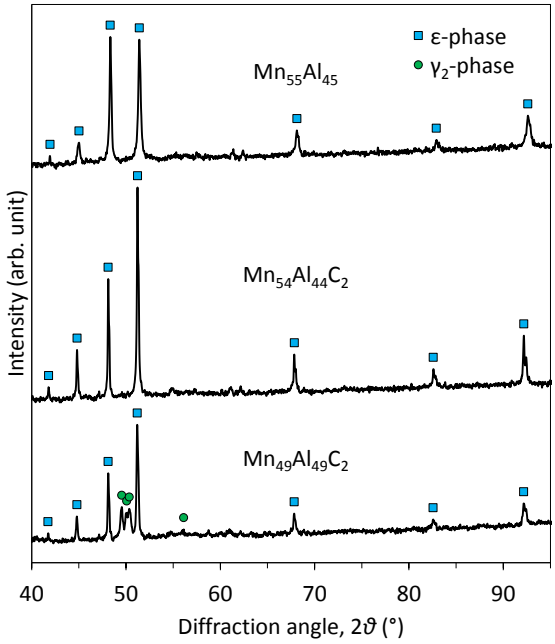

Figure 3. XRD patterns of melt-spun powders without thermal treatment. These precursors are mostly composed of ϵ-phase.

in $Mn_{54}Al_{44}C_2$ melt-spun sample after furnace annealing at 550 °C [15]. This may indicate that, despite high heating/cooling rate, the elevated sintering temperatures of 650–950 °C are not optimal for the structural $\epsilon \rightarrow \tau$ transition to occur without decomposition.

Addition of carbon slightly increases both lattice parameters of ϵ-phase, whereas in τ-phase it leads to decrease of a and pronounced ($\sim$1.5 %) increase of c, the unit cell volume also increases [15]. Though C has been reported to occupy $(\frac{1}{2}, \frac{1}{2}, \frac{1}{2})$ sites together with Al [20], this observation provides a new evidence for presence of carbon atoms in the interstitial positions $(0, 0, \frac{1}{2})$ and $(\frac{1}{2}, \frac{1}{2}, 0)$ of tetragonal τ-phase [11, 21] similar to Fe-C martensite.

The mean size of reflecting crystallites determined from line broadening is 80–160 nm for most phases. Exception is ϵ-phase having larger grains in as-quenched melt-spun samples due to a columnar microstructure. Lattice parameters and volume fraction of each phase have been used for calculation of a theoretical density to compare with the macroscopic density measured directly. The values of relative density in table 1 confirm the analysis of SPS curves. Bulk $Mn_{55}Al_{45}$ sample (containing no τ-phase) is fully densified, whereas in $Mn_{49}Al_{49}C_2$ and $Mn_{54}Al_{44}C_2$ samples (which experienced $\epsilon \rightarrow \tau$ transformation during SPS at 650 °C) the density is only $\sim$90 %. Thus, further investigation of the sintering mechanism in the presence of structural phase transformations is needed. A possible solution to this problem can be found by introducing a ball milling stage before SPS.

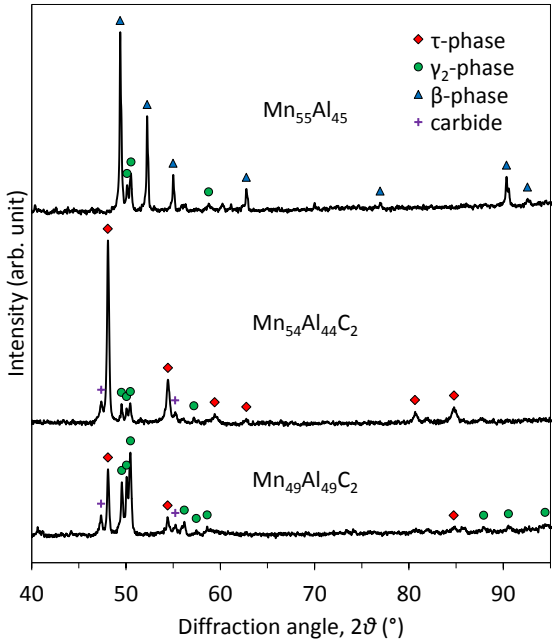

Figure 4. XRD patterns of sintered at 650 °C bulk samples. The $Mn_{54}Al_{44}C_2$ alloy contains more ferromagnetic τ-phase than other compositions.

Table 1. Nominal composition of the studied alloys, XRD phase analysis (weight fractions) of as-quenched (AQ), annealed at 550 °C and sintered at 650–950 °C samples, and relative density (measured directly / calculated from XRD data).

Composition (at.%)	State	Phases (wt.%)				Density (%)
		ϵ	τ	γ_2	β	
$Mn_{49}Al_{49}C_2$	AQ	59	–	41	–	–
	550	–	70	30	–	–
	650	–	25	67	–	92
	850	–	35	65	–	99
	950	–	46	54	–	99
$Mn_{54}Al_{44}C_2$	AQ	100	–	–	–	–
	550	–	100	–	–	–
	650	–	84	6	–	88
	850	–	79	21	–	100
	950	–	96	4	–	100
$Mn_{55}Al_{45}$	AQ	100	–	–	–	–
	550	–	75	–	25	–
	650	–	–	33	67	100

3.3. Magnetic properties

Magnetic measurements were performed on melt-spun ribbons (annealed in the furnace or during *in-situ* heating/cooling in VSM) and sintered bulk samples (table 2). The

Table 2. Magnetic properties of annealed at 550 °C melt-spun ribbons and sintered at higher temperatures (650–950 °C) bulk samples in applied field of 1.9 T.

Composition (at.%)	Temperature T_{ht} (°C)	Magnetization $\mu_0 M_s$ (T)	Remanence $\mu_0 M_r$ (T)	Coercivity $\mu_0 H_a$ (T)
$Mn_{49}Al_{49}C_2$	550	0.38	0.22	0.23
	650	0.15	0.08	0.31
	850	0.22	0.09	0.13
	950	0.24	0.09	0.10
$Mn_{54}Al_{44}C_2$	550	0.55	0.31	0.18
	650	0.50	0.26	0.19
	850	0.47	0.16	0.09
	950	0.59	0.14	0.05
$Mn_{55}Al_{45}$	550	0.43	0.24	0.14

room temperature magnetization curves of two compositions having ferromagnetic behaviour are presented in figure 5 and figure 6. These results agree well with XRD data (table 1) as τ-phase responsible for hard magnetism is observed after sintering only in $Mn_{49}Al_{49}C_2$ and $Mn_{54}Al_{44}C_2$. Moreover, there is a correlation between the weight fraction of τ-phase determined from XRD and the saturation magnetization value extracted from VSM measurements. The $Mn_{54}Al_{44}C_2$ alloy with major τ-phase shows higher magnetization and lower coercivity of 0.19 T. Two-phase alloy $Mn_{49}Al_{49}C_2$ with minor τ-phase shows lower magnetization and higher coercivity of 0.31 T. Our values of coercivity are higher than 0.17 T [7] and 0.15 T [8] reported for rapid solidification attempts, but lower compared to 0.48 T [11] achieved in a ball milled (not sintered) powder. Sintering at 650 °C gives better coercivity because of larger fraction of non-magnetic γ_2-phase, finer grains and increased porosity, which leads to formation of numerous pinning centres. Sintering at 850–950 °C results in higher density, more homogeneous phase distribution and less complex microstructure.

Figure 7 shows the magnetization of as-quenched $Mn_{54}Al_{44}C_2$ sample as a function of temperature in a constant magnetic field of 1.4 T. Thermal ramps were performed between 27 °C and 627 °C at 5 K/min rate. The precursor ϵ-phase is antiferromagnetic at low temperatures [22] and paramagnetic under normal conditions. On heating, ϵ-phase transforms to τ-phase which is also paramagnetic at the transition temperature ∼513 °C (see the inset). The structural transition is detected due to a difference in magnetic susceptibility of the phases involved. On cooling, the magnetization is increased drastically below the Curie temperature of τ-phase as the reverse transition to ϵ-phase does not occur, probably, due to kinetic reasons. In Mn-Al-C alloys the Curie temperature of τ-phase decreases with carbon doping, however available data largely vary [7, 8, 11]. Taking into account this dependence, we find a good agreement of our T_c measurements with results of Zeng *et al.* [11]. The coercivity of $Mn_{54}Al_{44}C_2$ sample subjected to *in-situ* annealing is 0.19 T, close to the values received after furnace annealing and low temperature SPS (Table 2).

Additional information on magnetization processes can be obtained from field-dependent remanence measurements. According to the Stoner-Wohlfarth theory, for a system of non-interacting single-domain particles the following relation holds true

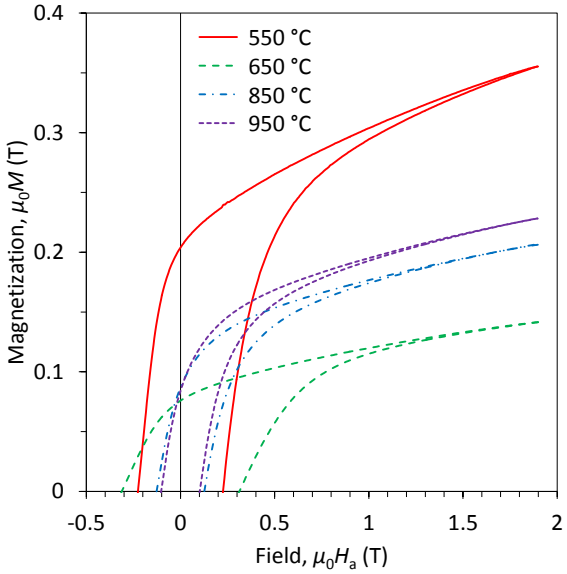

Figure 5. Magnetic hysteresis loops of $Mn_{49}Al_{49}C_2$ alloy at room temperature. The sintered at 650 °C sample shows higher coercivity but lower magnetization than the annealed at 550 °C ribbon due to a smaller content of τ-phase.

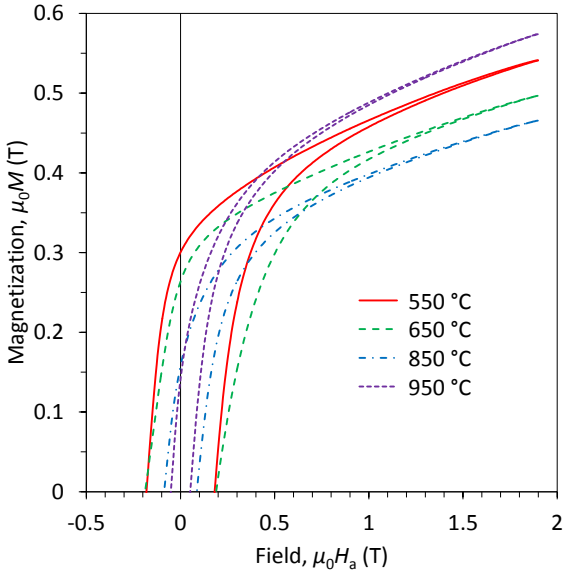

Figure 6. Magnetic hysteresis loops of $Mn_{54}Al_{44}C_2$ alloy at room temperature. The dependence of magnetic properties on heat treatment conditions is less pronounced compared to $Mn_{49}Al_{49}C_2$ alloy due to higher stability of τ-phase.

[23]:

$$\Delta m(H) \equiv 2m_r(H) + m_d(H) - 1 = 0. \quad (1)$$

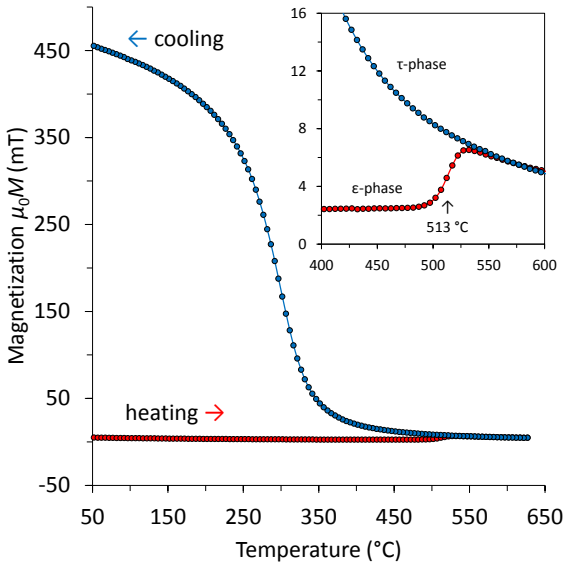

Figure 7. Magnetization as a function of temperature under applied magnetic field for as-quenched $Mn_{54}Al_{44}C_2$ sample. Inset: a magnified fragment of the curve showing the temperature induced $\epsilon \rightarrow \tau$ structural phase transition.

Here $m_r(H) \equiv M_r(H)/M_r(\infty)$ is the reduced initial remanence obtained by applying a magnetic field to the virgin state (IRM), $m_d(H) \equiv M_d(H)/M_r(\infty)$ is the reduced demagnetization remanence obtained in a reverse field after saturating the magnetization (DCD). Deviation parameter $\Delta m(H)$ serves as a measure of interaction between particles in real systems [24]. Positive values of $\Delta m(H)$ are due to interactions promoting the magnetized state, whereas negative values of $\Delta m(H)$ are caused by interactions tending to assist magnetization reversal. Similar relations between remanence curves can also be derived using the Preisach model of hysteresis [25].

For $Mn_{49}Al_{49}C_2$ and $Mn_{54}Al_{44}C_2$ alloys sintered at 650 °C, remanence curves $m_r(H)$ and $m_d(H)$ are presented in figure 8, deviation parameter $\Delta m(H)$ is plotted in figure 9. Two samples show similar initial remanence shape, whereas their demagnetization behaviour differs. The $Mn_{54}Al_{44}C_2$ alloy with high content of ferromagnetic τ-phase reveals regions of positive and negative $\Delta m(H)$ values, which can be explained by a competition of different dipolar or exchange interactions. The $Mn_{49}Al_{49}C_2$ alloy, which contains significant amount of non-magnetic phase and probably has a specific microstructure, exhibits much stronger magnetic interactions and positive $\Delta m(H)$ values. This behaviour can be attributed to higher density of pinning centres in the inhomogeneous material and is related to its higher coercivity.

4. Conclusion

Spark plasma sintering technique has been employed to produce solid Mn-Al-C permanent magnets from melt-spun ribbons. Simultaneous application of heat and pressure in the process of consolidation enabled us to eliminate the separate stage of annealing usually required for transformation of the parent ϵ-phase into the

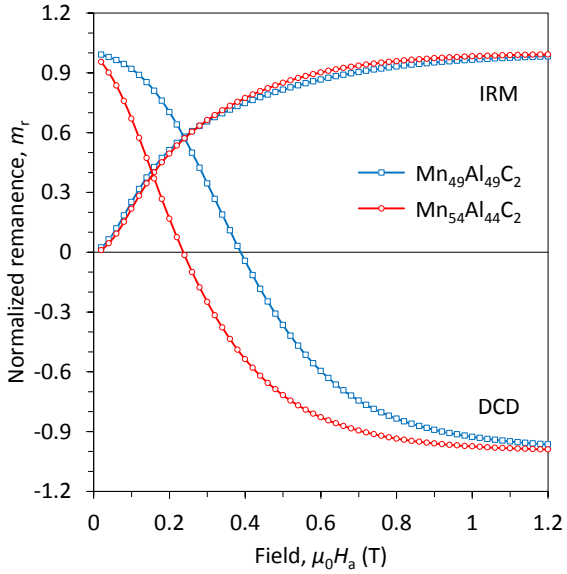

Figure 8. Reduced initial remanence m_r (IRM) and reduced demagnetization remanence m_d (DCD) as functions of applied magnetic field. The reversal behaviour differs for two compositions.

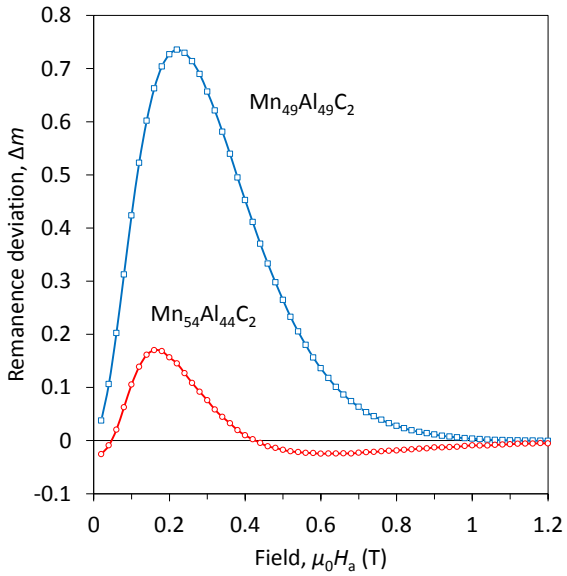

Figure 9. Reduced remanence deviation as a function of applied magnetic field calculated according to (1). The $Mn_{54}Al_{44}C_2$ alloy behaves more close to the system of Stoner-Wohlfarth particles than the $Mn_{49}Al_{49}C_2$ alloy.

ferromagnetic τ-phase. However, further optimization of the production parameters is necessary, including the choice of particle size and thermal regimes of sintering.

References

[1] J. M. D. Coey. Permanent magnets: Plugging the gap. *Scr. Mater.*, 67:524–529, 2012.

[2] H. Kono. On the ferromagnetic phase in manganese-aluminum system. *J. Phys. Soc. Jpn.*, 13:1444–1451, 1958.

[3] A. J. J. Koch, P. Hokkeling, M. G. van der Steeg, and K. J. de Vos. New material for permanent magnets on a base of Mn and Al. *J. Appl. Phys.*, 31:75S–77S, 1960.

[4] T. Ohtani, N. Kato, S. Kojima, K. Kojima, Y. Sakamoto, I. Konno, M. Tsukahara, and T. Kubo. Magnetic properties of Mn-Al-C permanent magnet alloys. *IEEE Trans. Magn.*, 13:1328–1330, 1977.

[5] J. M. K. Wiezorek, A. K. Kulovits, C. Yanar, and W. A. Soffa. Grain boundary mediated displacive-diffusional formation of τ-phase MnAl. *Metall. Mater. Trans. A*, 42:594–604, 2011.

[6] Y. Sakka, M. Nakamura, and K. Hoshimoto. Rapid quenching and properties of hard magnetic materials in MnAl-X (X = Ti, Cu, Ni, C, B) systems. *J. Mater. Sci.*, 24:4331–4338, 1989.

[7] E. Fazakas, L. K. Varga, and F. Mazaleyrat. Preparation of nanocrystalline Mn-Al-C magnets by melt spinning and subsequent heat treatments. *J. Alloy. Compd.*, 434–435:611–613, 2007.

[8] Z. W. Liu, C. Chen, Z. G. Zheng, B. H. Tan, and R. V. Ramanujan. Phase transitions and hard magnetic properties for rapidly solidified MnAl alloys doped with C, B, and rare earth elements. *J. Mater. Sci.*, 47:2333–2338, 2012.

[9] Y. J. Kim and J. H. Perepezko. Formation of a metastable ferromagnetic τ phase during containerless melt processing and rapid quenching in Mn-Al-C alloys. *J. Appl. Phys.*, 71:676–680, 1992.

[10] A. E. Berkowitz, J. D. Livingston, and J. L. Walter. Properties of Mn-Al-C magnets prepared by spark erosion and other rapid solidification techniques. *J. Appl. Phys.*, 55:2106–2108, 1984.

[11] Q. Zeng, I. Baker, J. B. Cui, and Z. C. Yan. Structural and magnetic properties of nanostructured Mn-Al-C magnetic materials. *J. Magn. Magn. Mater.*, 308:214–226, 2007.

[12] J.-G. Lee, X.-L. Wang, Z.-D. Zhang, and C.-J. Choi. Effect of mechanical milling and heat treatment on the structure and magnetic properties of gas atomized Mn-Al alloy powders. *Thin Solid Films*, 519:8312–8316, 2011.

[13] T. Saito. Magnetic properties of Mn-Al-C alloy powders produced by mechanical grinding. *J. Appl. Phys.*, 97:10F304, 2005.

[14] Z. A. Munir, U. Anselmi-Tamburini, and M. Ohyanagi. The effect of electric field and pressure on the synthesis and consolidation of materials: A review of the spark plasma sintering method. *J. Mater. Sci.*, 41:763–777, 2006.

[15] A. Pasko, F. Mazaleyrat, M. LoBue, E. Fazakas, and L. K. Varga. Hard magnetic properties of melt-spun Mn-Al-C alloys. *Eur. Phys. J. Web Conf.*, 40:06008, 2013.

[16] L. Lutterotti. Maud: a Rietveld analysis program designed for the internet and experiment integration. *Acta Crystallogr. A*, 56:s54, 2000.

[17] D. M. Hulbert, A. Anders, D. V. Dudina, J. Andersson, D. Jiang, C. Unuvar, U. Anselmi-Tamburini, E. J. Lavernia, and A. K. Mukherjee. The absence of plasma in "spark plasma sintering". *J. Appl. Phys.*, 104:033305, 2008.

[18] R. Orrù, R. Licheri, A. M. Locci, A. Cincotti, and G. Cao. Consolidation/synthesis of materials by electric current activated/assisted sintering. *Mater. Sci. Eng. R*, 63:127–287, 2009.

[19] A. Shukla and A. D. Pelton. Thermodynamic assessment of the Al-Mn and Mg-Al-Mn systems. *J. Phase Equilib. Diffus.*, 30:28–39, 2009.

[20] J.-L. Yang, H.-M. Zhou, J.-X. Zhu, X.-X. Zeng, B.-S. Zhang, and L. Jin. Neutron diffraction study of hard magnetic alloy MnAlC. *J. Appl. Phys.*, 55:2053–2054, 1984.

[21] C. T. Lee, K. H. Han, I. H. Kook, and W. K. Choo. Phase and lattice parameter relationships in rapidly solidified and heat-treated $(Mn_{0.53}Al_{0.47})_{100-x}C_x$ pseudo-binary alloys. *J. Mater. Res.*, 7:1690–1695, 1992.

[22] J. J. Wysłocki, P. Pawlik, and A. Przybył. Magnetic properties of the non-oriented ϵ-phase in Mn-Al-C permanent magnet. *Mater. Chem. Phys.*, 60:211–213, 1999.

[23] E. P. Wohlfarth. Relations between different modes of acquisition of the remanent magnetization of ferromagnetic particles. *J. Appl. Phys.*, 29:595–596, 1958.

[24] P. E. Kelly, K. O'Grady, P. I. Mayo, and R. W. Chantrell. Switching mechanisms in cobalt-phosphorus thin films. *IEEE Trans. Magn.*, 25:3881–3883, 1989.

[25] V. Basso, M. Lo Bue, and G. Bertotti. Interpretation of hysteresis curves and Henkel plots by the Preisach model. *J. Appl. Phys.*, 75:5677–5682, 1994.